HHS Public Access

Author manuscript

Nat Electron. Author manuscript; available in PMC 2024 August 01.

Published in final edited form as:

Nat Electron. 2024 February ; 7(2): 168–179. doi:10.1038/s41928-023-01116-6.

A physicochemical-sensing electronic skin for stress response monitoring

Changhao Xu[1,5], **Yu Song**[1,5], **Juliane R. Sempionatto**[1,5], **Samuel A. Solomon**[1,5], **You Yu**[1], **Hnin Y. Y. Nyein**[2], **Roland Yingjie Tay**[1], **Jiahong Li**[1], **Wenzheng Heng**[1], **Jihong Min**[1], **Alison Lao**[1], **Tzung K. Hsiai**[3], **Jennifer A. Sumner**[4], **Wei Gao**[1,*]

[1]Andrew and Peggy Cherng Department of Medical Engineering, Division of Engineering and Applied Science, California Institute of Technology, Pasadena, CA, USA.

[2]Department of Chemical and Biological Engineering, Hong Kong University of Science and Technology, Hong Kong, China.

[3]Division of Cardiology, David Geffen School of Medicine, University of California, Los Angeles, CA, USA.

[4]Department of Psychology, University of California, Los Angeles, CA, USA.

[5]These authors contributed equally to this work.

Abstract

Approaches to quantify stress responses typically rely on subjective surveys and questionnaires. Wearable sensors can potentially be used to continuously monitor stress-relevant biomarkers. However, the biological stress response is spread across the nervous, endocrine, and immune systems, and the capabilities of current sensors are not sufficient for condition-specific stress response evaluation. Here we report an electronic skin for stress response assessment that non-invasively monitors three vital signs (pulse waveform, galvanic skin response and skin temperature) and six molecular biomarkers in human sweat (glucose, lactate, uric acid, sodium ions, potassium ions and ammonium). We develop a general approach to prepare electrochemical sensors that relies on analogous composite materials for stabilizing and conserving sensor interfaces. The resulting sensors offer long-term sweat biomarker analysis of over 100 hours with high stability. We show that the electronic skin can provide continuous multimodal physicochemical monitoring over a 24-hour period and during different daily activities. With the help of a machine learning pipeline, we also show that the platform can differentiate three stressors with an accuracy of 98.0%, and quantify psychological stress responses with a confidence level of 98.7%.

* weigao@caltech.edu.

Author contributions

W.G. and C.X. conceived the project. C.X. led the sensors and CARES platform development. C.X., Y.S. and J.R.S. led the platform characterization and human studies. S.A.S. and J.L. contributed to the data processing and feature extraction. H.Y.Y.N. contributed to sensor development. Y.Y., R.Y.T., and A.L. contributed to sensor characterization and test. W.H. and J.M. contributed to wireless system development. T.K.H. and J.A.S. contributed to the human study design. W.G., C.X., Y.S., J.R.S. and S.A.S. co-wrote the paper. All authors contributed to the data analysis and provided the feedback on the manuscript.

Competing interests: Authors declare no competing interests.

Stress is a process triggered by demanding physical or psychological events, and may cause anxiety as a prototypical psychological response. While acute stress responses in healthy individuals can be adaptive and manageable, persistent experiences of stress can have deleterious impacts on mental and physical health[1,2], and many mechanisms behind the stress response are yet unknown[3,4] (Supplementary Note 1). In the United States alone, over 50 million adults suffer from depression, and after the onset of the COVID-19 pandemic, the number of people suffering from mental disorders has drastically risen, causing a heavy burden on the healthcare system[5,6]. Elevated levels of stress and anxiety also pose a large burden to high-demand occupation workers[7], such as athletes[8], soldiers[9], first responders[10], and aviation personnel[11], potentially interfering with their cognitive performance and decision-making process[12]. In response to these impacts, understanding and evaluating the stress response has become a cornerstone of clinical healthcare. However, current gold standards for clinical stress response assessments rely on surveys and performance evaluations, which can be highly subjective[13-15]. Thus, there exists a pressing demand for developing a more efficient and effective stress assessment tool that is not characterized by these limitations[16,17].

Non-invasive biomarkers present themselves as a reliable alternative for monitoring the stress response due to the interdependencies between biological and psychological stress. In particular, stress induces a complex biological response within the nervous, endocrine, and immune systems (Fig. 1a)[18,19]. The perception of stress activates the hypothalamic-pituitary-adrenal (HPA) axis and sympathetic adrenal medullary (SAM) axis from the hypothalamus in the brain. Acetylcholine in nerve fibers from both axes will stimulate the adrenal gland, releasing stress hormones (e.g., epinephrine, norepinephrine, and cortisol) into the blood. Acetylcholine can also activate sudomotor neurons connected to sweat glands that release ion-rich fluids. This sympathetic activity can be indirectly measured through the galvanic skin response (GSR) and sweat electrolyte levels[20]. The released stress hormones inhibit insulin production, affecting the synthesis of metabolites such as glucose, lactate, and uric acid (UA), as well as narrow arteries, boosting cardiac activities. By monitoring these stress-relevant biomarkers, it is possible to develop a comprehensive and objective health profile relating biophysical and biochemical signals to dynamic stress response monitoring[21-23].

Recent advances in wearable sensors have enabled real-time and continuous monitoring of physical vital signs[24-28], allowing for a more personalized remote healthcare. Through *in situ* human sweat analysis, wearable biosensors can provide insightful information on an individual's health at the molecular level[29-32]. Despite these promising prospects, major challenges of these sensors exist for clinical applications: a limited set of physical signals are not sufficient for condition-specific assessment of psychological and physiological stress[33]; existing wearable biochemical sensors suffer from poor operational stability in biofluids, which precludes reliable long-term continuous monitoring[34]; the access to human sweat usually requires physical activity that can affect an individual's stress; despite recent progress on stress hormone analysis, continuous monitoring of sweat stress hormones at physiologically-relevant levels using wearable sensor has not yet been achieved due to their extremely low concentrations[35-37]. Therefore, while understanding and monitoring the endocrine response to stress is a promising approach, it is still underdeveloped.

We report here a consolidated artificial intelligence-reinforced electronic skin (CARES) with robust long-term sensing capabilities for stress response monitoring (Fig. 1a). Fabricated via a scalable inkjet-printing approach, the wearable device is capable of multiplexed, non-invasive monitoring of key stress-related physiological signals – pulse waveform, GSR, and skin temperature – along with sweat metabolites – glucose, lactate, and UA – as well as electrolytes – Na^+, K^+, and NH_4^+ – during daily activities (Fig. 1b,c). Through the integration of a miniaturized iontophoresis module, sweat can be induced autonomously at rest without the need for vigorous exercise. We introduce a general approach to prepare highly stable and sensitive electrochemical biosensors, which utilizes analogous composite materials for stabilizing and conserving sensor interfaces. The obtained biochemical sensors achieved a record-breaking long-term stability of more than 100 hours of continuous operation with minimal signal drifts (amperometric signals decaying less than 0.07% h^{-1} and potentiometric signals drift less than 0.04 mV h^{-1}), which greatly exceeds those obtained with previous widely adopted wearable sweat sensors. Built on an ultrathin flexible polyimide substrate (4 μm) for flexibility and robustness as well as integrated with microfluidics, the CARES device conformally laminates on the wrist for reliable and robust sensing (Fig. 1d,e). This allows for 24-hour continuous monitoring of daily activities, yielding greater insight into how these signals vary throughout the day. With a machine learning (ML) pipeline incorporating previously inaccessible multimodal data (Fig. 1f), we demonstrate that the physicochemical sensor data obtained by the wearable technology can not only be used to classify responses to stressors at high accuracies, but also predict state anxiety levels (a key psychological response to stress) with high reliability.

The CARES platform

The CARES platform consists of a multi-layered sensor patch and a skin-interfaced laser-engraved microfluidic module (Fig. 1d,e). The sensor patch contains carbachol hydrogel (carbagel)-loaded sweat stimulation electrodes, three enzymatic biosensors, three ion-selective sensors, a capacitive pulse sensor, a resistive GSR sensor, and a skin temperature sensor. The platform can be mass-fabricated through serial inkjet printing of silver and carbon as the interconnects and electrodes for top and bottom layers (Supplementary Fig. 1). A middle polydimethylsiloxane (PDMS)-based airgap layer was spin coated between top and bottom layers, as the soft PDMS facilitates pulse pressure sensitivity and sweat reservoir collection. The microfluidic module was assembled in a sandwiched structure (PDMS/polyethylene terephthalate/medical tape) and contains two separate reservoirs (Supplementary Figs. 2 and 3) that enable fresh sweat sampling and rapid refreshing for accurate sweat analysis with high temporal resolution. Carbachol was used for sweat induction as it enables long-lasting sudomotor axon reflex sweat secretion from the surrounding sweat glands owing to its nicotinic effects[38]. In this work, six molecular biomarkers (glucose, lactate, UA, Na^+, K^+, and NH_4^+) were selected as the detection targets due to their strong associations with stress responses (Supplementary Note 2)[39-43]. Together with laser-patterned microfluidics, the CARES device can be attached to the subject's wrist comfortably and performs multiplexed metabolic sensing *in situ*.

Wearable sensors for long-term continuous operation

A number of electrochemical sensing strategies based on enzymes[29], ionophores[44], molecularly imprinted polymers[30], aptamers[45], and antibodies[46] are reported, where the majority of existing wearable chemical sensors are primarily based on amperometric enzymatic sensors or potentiometric ion-selective electrodes (ISEs) as these sensors could offer real-time continuous monitoring with high temporal resolution. However, one main bottleneck for the practical applications of these sensors is their limited operation lifetime and long-term stability during continuous wearable sensing. Large sensor drifts are evident when they are used in body fluids which substantially hinder the long-term continuous usability of wearable chemical sensors.

Most wearable enzymatic biosensors are based on Prussian blue (PB), which serves as an efficient electron-transfer mediator with a low redox potential of around 0 V. However, PB-based biosensors suffer from poor stability during long-term use in biofluids because PB degrades in neutral and alkaline solutions as the hydroxide ions (OH^-), a product of H_2O_2 reduction, can break the Fe—(CN)—Fe bond (Supplementary Note 3). In order to stabilize PB while retaining its catalytic activity, we utilize a PB-analogue nickel hexacyanoferrate (NiHCF) with a similar zeolitic crystal structure that is catalytically inactive but forms a stabilized solid solution composite, protecting the PB sensor interface (Fig. 2a). Additionally, the enzymes were protected in a glutaraldehyde-crosslinked bovine serum albumin (BSA) matrix. To fabricate enzymatic sensors, gold nanoparticles (AuNPs) were electrodeposited onto an inkjet-printed inert carbon electrode to possess a high electroactive area for sensitive electrochemical sensing followed by PB-NiHCF deposition. Scanning transmission electron microscopy (STEM) and energy dispersive spectroscopy (EDS) analyses (Fig. 2b and Supplementary Fig. 4) indicate that NiHCF forms a thin protective layer on PB with an obscure boundary. Our electrochemical characterizations confirmed that, compared to PB which suffered from rapid degradation during electrochemical measurement and other transition metal hexacyanoferrates (i.e., PB-CoHCF and PB-CuHCF), PB-NiHCF could withstand pH corrosion and maintain most consistent electrochemical catalytic activity (Supplementary Figs. 5-7). This could be attributed to two mechanisms (Supplementary Note 3): 1) nickel is inert compared with iron and can withstand OH^- group corrosion (Supplementary Fig. 8); 2) Ni ion has a smaller ionic radius compared to other transitional metal ions (such as Co and Cu ions), which is preferred to withstand ion insertion (Supplementary Fig. 9). Both mechanisms were further supported with scanning electron microscope (SEM) characterizations of the electrodes (Supplementary Fig. 10) and inductively coupled plasma–mass spectrometry (ICP–MS) analysis of the dissolved Fe^{2+} from the electrodes (Supplementary Fig. 11) before and after electrochemical tests. These results indicated that PB dissolved after tests under different pHs and repetitive CV scans, while NiHCF didn't show any substantial degradation and maintained the highest stability among the transition metal hexacyanoferrates for PB stabilization.

Highly stable, continuous, and selective monitoring of sweat glucose, lactate, and UA was realized amperometrically, and a linear response between current output and target concentrations was obtained for all three sensors in physiologically relevant concentration

ranges over a 25-hour evaluation period (Fig. 2c). The sensitivities for glucose, lactate, and UA sensors were 33.65 nA μM^{-1} cm^{-2}, 185.56 nA mM^{-1} cm^{-2}, and 26.36 nA μM^{-1} cm^{-2}, respectively. These sensors also showed a record-breaking long-term stability of more than 100 hours of continuous operation in phosphate buffered saline (PBS) solutions and untreated human sweat samples, which greatly exceeded those obtained with previous widely adopted wearable sweat sensors (Supplementary Fig. 12, Supplementary Fig. 13, and Supplementary Table 1). It should be noted that as sweat lactate is present in high concentrations (up to 60 mM), an additional diffusion-limited polyvinyl chloride (PVC)/ bis(2-ethylhexyl) sebacate (DOS) membrane was introduced on top of the enzyme film to achieve a wide linear range while maintaining high sensor stability (Supplementary Fig. 14).

Existing wearable ISEs are based on PVC/DOS membranes and are plagued with a potential drift of typically ~2 mV h^{-1} over time, which is attributed to ionophore leaching and water formation below the ion-selective membrane[47]. To address this issue during long-term operation, we adopted another analogous composite materials design strategy by introducing polystyrene-block-poly (ethylene butylene)-block-polystyrene (SEBS) into the PVC system, which shares a similar long-chain structure but holds more methyl and phenyl groups at the sensor interface to promote hydrophobicity and mechanical strength (Fig. 2d). High hydrophobicity suppresses ionophore leaching and prevents water layer formation at the interface. To fabricate ISEs, the inert yet high surface area nature of inkjet-printed carbon nanoparticle electrodes was utilized without the need to deposit additional ion-charge transducer materials. Ion-selective membranes based on the PVC-SEBS matrix were dropcasted onto the carbon electrode, and the ratio of SEBS-PVC was evaluated to identify the optimal stability (Fig. 2e, Supplementary Note 4). The optimized ISEs could obtain prolonged stability of 100 hours of continuous operation in both standard solutions and human sweat samples with the potential value decaying less than 0.04 mV h^{-1} (Supplementary Fig. 15, Supplementary Fig. 16, and Supplementary Table 2). A logarithmic-linear relationship between the potentiometric output of Na^+, K^+ and NH_4^+ with near-Nernstian sensitivities of 58.9, 60.6 and 61.2 mV per decade respectively was identified during a 25-hour prolonged sensor evaluation in physiologically relevant ranges (Fig. 2f and Supplementary Fig. 17).

With an analogous composite materials' approach, our sensors demonstrated high reproducibility (Supplementary Fig. 18), selectivity (Supplementary Fig. 19), and long-term continuous operation stability in both standard solutions and untreated human sweat over multiple days (Supplementary Figs. 12, 13, 15 and 16). Such sensor performance, to the best of our knowledge, was among the best in wearable sweat sensing (Supplementary Tables 1 and 2). The low-cost mass-producible sensor patch is designed to be disposable after use: the anticipated wearable usage time for each patch is 24–48 hours and the users could easily replace the sensor patch. Thus, our sensors can provide a stable response longer than the expected wearable usage time. The general material strategy demonstrated here, based on electrodes prepared by inkjet printing, can be applicable to electrodes manufactured by other scalable technologies including laser engraving and thin-film evaporation (Supplementary Fig. 20). In addition, the sensor preparation approach here is also not limited to the six sensors we proposed in this study; it can serve as a universal and readily reconfigurable

method for other enzymatic and ionophore-based biosensors toward a broad range of practical applications.

To realize practical molecular biomarker monitoring without the need for vigorous exercise, miniaturized iontophoresis electrodes coated with carbagels were incorporated into the CARES for autonomous, local sweat induction (Fig. 2g). Sweat can be continuously secreted from the surrounding glands over a prolonged period of time due to the nicotinic effects of carbachol (transdermally delivered for 5 minutes via a small 50 μA current). Efficient sampling was obtained through custom-developed microfluidics for real-time bioanalysis with high temporal resolution (Fig. 2h, Supplementary Figs. 21 and 22, Supplementary Video 1).

In addition to chemical sensors, the CARES also contains multiple physical sensors to monitor stress-related vital signs. We placed a capacitive pressure sensor above the radial artery for pulse waveform monitoring (Fig. 2i). Because of the soft PDMS-engraved airgap, the pressure sensor is highly sensitive to soft pressure loads (such as a feather), with an impressive sensitivity of 113.1% kPa^{-1} under the range of 0–500 Pa (Fig. 2j,k). The pressure sensor also displays highly robust performance and mechanical stability during a repetitive pressure-loading test involving 5,000 cycles, mimicking daily use on the skin (Supplementary Fig. 23). A printed resistive temperature sensor was integrated into the CARES for skin temperature recording *in situ* with a sensitivity around 0.115% $°C^{-1}$ in physiological temperature ranges between 25–50 °C (Fig. 2l and Supplementary Fig. 24). Considering that temperature has a strong influence on enzymatic activities, the temperature information is used for calibrating the response of the three enzymatic biosensors to achieve highly accurate *in situ* metabolic analysis (Supplementary Figs. 25 and 26). It should be noted that other environmental factors such as humidity showed minimal influence on the performance of our chemical sensors (Supplementary Fig. 27). Additionally, a pair of printed Ag electrodes were used as a GSR sensor which demonstrated high conductivity compared with commercial gel electrodes (Fig. 2m). Owing to the ultrathin flexible polyimide substrate and strong interfacial strength enabled by the medical adhesive, the CARES showed excellent skin contact and mechanical resilience against undesirable physical deformations during continuous operations (Supplementary Figs. 28 and 29). The impermeable polyimide packaging also eliminated the influence of humidity from environmental surroundings and sweat (Fig. 2n).

Continuous daily monitoring across various activities

Owing to the excellent long-term stability of wearable sweat biosensors, the CARES enables long-term real-time continuous monitoring of physicochemical biomarkers. As illustrated in Fig. 3a, the CARES can successfully record the dynamic changes of metabolites and vital signs over 24-hours of activity, involving casual and vigorous exercise, dietary intakes, lab work, relaxing entertainment, and sleep. Glucose and UA levels spiked after food intake, indicating rapidly increased metabolic activities. During vigorous exercise, substantial increases in vascular activity and skin electrolyte/conductivity were observed, and stable output for both metabolites and vital signs were detected during sleep at night.

Such powerful capabilities of continuous multimodal monitoring will enable a number of personalized healthcare and human performance monitoring applications.

Machine learning approach for stress evaluation

To evaluate the use of the CARES for stress response monitoring, controlled experiments were performed on ten healthy subjects using three different physiological and psychological stressors, namely the cold pressor test (CPT), a virtual reality challenge (VR), and intense exercise (Supplementary Note 5). The dynamic profiles of all individual sensors integrated in the CARES were collected during each study, as illustrated in Fig. 3b-d and Supplementary Figs. 30-33. State anxiety levels, as measured by the State-Trait Anxiety Inventory (STAI-Y) questionnaire with scores ranging between 10 – 40 points (10 indicating little to no anxiety)[48], were the psychological stress response measure for data training (Supplementary Note 6). The questionnaire was administered before and after each stressor to quantify the induced anxiety levels within a subject (Supplementary Fig. 34).

For each experiment, on-body chemical and physical data showed significant variations in response to each stressor. During the CPT experiment, the subjects immersed one hand in ice water for 3 minutes. A natural reaction of vasoconstriction occurred where the blood vessel constricted in response to cold temperatures[49]. As a result, immediate physiological responses including altered pulse waveform and elevated GSR were observed, consistent with previous reports on the variations of physiological signals with cold-stimulated stress response[50,51]. In addition, delayed mild fluctuations in metabolite concentrations of glucose, lactate, and UA from some subjects were also observed. During the VR test, subjects wore an Oculus VR headset to play a rhythm game (Beat Saber) while the gaming screen was mirrored to a computer monitor with an audience, resulting in both physiological and social-evaluative psychological stress. We observed substantial differences in the pulse waveform and GSR amplitude during and after the stress stimulus, along with elevated glucose, lactate and UA levels minutes later[39-41]. During vigorous exercise, profound activation of the HPA axis led to dramatic changes of all physiological signals as well as sweat metabolites and electrolytes (e.g., Na^+), in agreement with previous studies on exercise induced stress response[42,52]. These results indicate that the CARES can monitor stress-induced biological signals reliably.

To quantify the stress response-related features, data-driven stress and anxiety evaluation were performed after each experiment was complete, where an ML pipeline was developed to extract features and deconvolute connections between physicochemical information and stressor types and state anxiety levels (Fig. 4a and Supplementary Note 7). We undertook this challenge using three separate ML analyses: stress detection versus relaxation, stressor classification, and anxiety level evaluation, where we trained and tested each model across three experiments (VR, CPT, exercise) of all ten subjects for a total of 60,000 s of physiological CARES signals. All signals were calibrated and normalized to ensure that the features extracted after data pre-processing were stable against patch variations and any moderate motion artifacts (Supplementary Figs. 35-37, Supplementary Note 8, and Supplementary Table 3). Feature extraction was validated before ML analysis through projecting the multidimensional feature-space into 2D space via t-distributed

stochastic neighbor embedding (t-SNE)[53], where data from stress/relaxation naturally formed distinctive clusters, indicating the discriminative power of the features (Fig. 4b, Supplementary Fig. 38a).

Different ML models were evaluated, and the trained boosting decision tree model Extreme Gradient Boosting (XGBoost) outperformed typical ML models, including linear and radial basis function (RBF) support vector machines (SVM), logistic and ridge regression, and conventional decision trees (Fig. 4c). Combined with features extracted from both physiological and metabolic data, it was found that our XGBoost ML model could yield a much higher accuracy, with stress response classification accuracy of 99.2% for stress/relaxation detection (Supplementary Fig. 38) and an accuracy of over 98.0% for stressor classification, which to the best of our knowledge is the highest accuracy reported for stressor classification (Fig. 4d, Supplementary Table 4). It should be noted that differentiating stressors has high significance, as each stressor carries varying physiological and psychological influences and could act as risk factors for coping responses and cardiovascular diseases[54-56]. Distinguishing types of stressors has been recognized as a necessary condition for understanding the complex interrelationships among distinct stress experiences, as well as the collective impacts of stress on mental health[57] (Supplementary Note 5). Moreover, it resulted in highly consistent overall accuracies of over 99.3% across different individuals (Fig. 4e, Supplementary Note 9).

The Pearson correlation coefficients between all sensors in the CARES show the interrelatedness between physiological and chemical biomarkers (Fig. 4f). The relatively homogeneous correlation shows the high independence of the extracted features. To evaluate each physicochemical sensor's contribution to the model, feature importance of each biomarker towards each stressor was evaluated using a Shapley additive explanation (SHAP) (Fig. 4g, Supplementary Fig. 39, and Supplementary Note 9). Through SHAP analysis, the feature importance of GSR, pulse, glucose, and Na^+ indicate these biomarkers play a significant role in stressor classification. These results support the fact that stress responses involve participants' vascular dynamics, neural stimulation, and metabolism.

Based on the classification results, we expanded our analysis to state anxiety level evaluation. We adopted a similar XGBoost regression model and could predict state anxiety levels with a high confidence level of 98.7% and 98.1% coefficient of determination of scores from the STAI-Y (with a standard deviation of 4 points or less[48]) (Fig. 4h, Supplementary Note 6). The relevance of each feature was evaluated using SHAP analysis as well (Fig. 4i,j). Through SHAP analysis, it was determined that GSR, pulse, Na^+, K^+, and lactate played the most important role in state anxiety level prediction. Note that SHAP values show the relative significance of each feature in the ML model. Additionally, given the intrinsic limitations of questionnaires being able to only characterize state anxiety levels within a given time period rather than dynamic stress change continuously, we analyzed the stress response event as a whole to mimic questionnaire functionalities (Supplementary Note 3). In this circumstance, features were extracted from the stress region by taking mean signal changes from the moving average (MA) of sensor data rather than segmented at each timepoint, and a simple linear regression model was trained with fewer features selected to correspond to questionnaire scores and prevent overfitting (Supplementary Fig.

40). With the reduced size of dataset and analyzing the overall sensor responses in CARES, we performed a brute force feature selection within each biomarker and found that combined physicochemical features outperformed that of physical and chemical sensors alone.

To realize convenient data collection for real-life applications, in addition to using flexible cables connecting the CARES patch with laboratory instruments (Supplementary Fig. 41), we further designed a fully integrated wearable CARES system with a flexible printed circuit board (PCB) for multiplexed and multimodal signal processing as well as Bluetooth wireless communication (Supplementary Figs. 42-44). The wireless system was successfully used for on-body tests and validation of our CARES systems in the laboratory settings (Supplementary Fig. 45) and in real-life daily casual activities (Supplementary Fig. 46 and Supplementary Video 2). Our ML models obtained from the laboratory tests were able to accurately classify the types of stressors and state anxiety levels based on the wirelessly collected sensor data in the laboratory (Supplementary Fig. 47) as well as real-life settings (Supplementary Fig. 48). We anticipate that for large-scale human trials, the CARES will surpass the current gold standards for stress response quantification, and provide a highly robust stress response monitoring tool that is not reliant on subjective reporting with its potential for errors. In this regard, we envision a high potential for wearable multimodal physicochemical monitoring of dynamic stress response.

Conclusions

Here we have presented a CARES platform that performs multiplexed monitoring of key physiological signals, metabolites, and electrolytes simultaneously during a prolonged operation. Through materials engineering by applying analogous composite materials for stabilizing and conserving sensor interfaces, a general approach was developed to prepare highly stable and sensitive biochemical sensors including both enzymatic and ISE sensors, which has achieved a record-breaking long-term stability of more than 100-hour continuous operation with negligible sensor degradation. Continuous 24-hour monitoring of prolonged daily activities was also obtained. Real-time multimodal data of the stress response was generated from three different stressors utilizing both robust biochemical signals alongside physiological ones. With much-enhanced reliability of sensor readings, we demonstrate that both 1) a state of stress vs. relaxation and 2) state anxiety as a key psychological response to stress can be classified and predicted through multimodal health profiles at the metabolic level, with the capability of detecting and classifying stressor types at an accuracy of over 98.0% and evaluating state anxiety levels at a confidence level of 98.7%. We envision that by capturing a broader range of signals through more integrated biosensors, a more complete metabolic profile can be achieved for next-generation healthcare and human performance monitoring. Our CARES could pave the way for numerous practical wearable applications such as intelligent healthcare and personalized medicine.

Methods

Materials

The polystyrene-block-poly (ethylene butylene)-block-polystyrene (SEBS, Tuftec™) was provided by the Asahi Kasei Corporation. Uric acid (UA), sodium tetraphenylborate

(NaTPB), and glutaraldehyde (25% aqueous solution) were purchased from Alfa Aesar. Agarose, carbachol, bovine serum albumin (BSA), gold chloride trihydrate, hydrochloric acid, iron(III) chloride, potassium ferricyanide (III), potassium ferrocyanide (IV), polyvinyl chloride (PVC), polyvinyl butyral (PVB), bis(2-ethylhexyl) sebacate (DOS), 3,4-ethylenedioxythiophene (EDOT), poly(sodium 4-styrenesulfonate) (PSS), aniline, L-lactic acid, sodium ionophore X, sodium tetrakis[3,5-bis(trifluoromethyl) phenyl] borate (Na-TFPB), valinomycin, nonactin, tetrahydrofuran (THF), toluene, glucose oxidase from Aspergillus niger (216 U mg^{-1}), uricase from Bacillus fastidiosus (15.6 U mg^{-1}) were purchased from Sigma-Aldrich. Methanol, ethanol, sodium chloride, potassium chloride, nickel chloride, urea, L-ascorbic acid, dextrose (D-glucose) anhydrous, phosphate buffered saline (PBS) were purchased from Thermo Fisher Scientific. Lactate oxidase (106 U mg^{-1}) was purchased from Toyobo Co. Medical tapes (M-tapes) were purchased from 3M (468 MP). Polyethylene terephthalate (PET) films (12 μm thick) were purchased from McMaster-Carr. Polyimide (PI-2611) was purchased from HD MicroSystems, Inc. Polydimethyl siloxane (PDMS, SYLGARD 184) was purchased from Dow Corning. PI film (12.5 μm) was purchased from DuPont. STAI questionnaire license was purchased from Mind Garden, Inc.

Fabrication and assembly of the CARES device

CARES patch fabrication: The fabrication process of the CARES is illustrated in Supplementary Figs. 2 and 3. Polyimide was spin-coated on the silicon oxide wafer at a speed of 5000 rpm for 30 s and then cured at 350 °C for 1 hour with a ramping speed of 4 °C min^{-1}. The resulting polyimide substrate thickness is about 4 μm. For mass-fabrication, 12.5 μm PI film was used for large-area patterning demonstration. The CARES patch was then patterned with sequential printing of silver (interconnects and pin connections, reference electrode, pulse sensor, and galvanic skin response (GSR) sensor), carbon (iontophoresis electrodes, counter electrode, temperature sensor, working electrodes for biosensors), and polyimide (encapsulation) using an inkjet printer (DMP-2850, Fujifilm). The CARES patch was then annealed at 250 °C for 1 hour. A 1:12 mixture of curing agent to PDMS elastomer was prepared and stirred thoroughly for 10 minutes, after which the solution was spin-coated at the speed of 800 revolutions per minute (rpm) for 30 s onto the inkjet-printed bottom layer of CARES patch directly, followed by curing at 60 °C for 1 h. The resulting PDMS thickness is about 120 μm. Both the bottom layer and the top layer of the CARES patch were then laser patterned to define outlines and sweat outlets using a 50 W CO_2 laser cutter (Universal Laser System) with power 25%, speed 50%, pulse per inch (PPI) 1000 in vector mode. The bottom layer was further cut to define iontophoresis reservoirs, sweat reservoirs, and airgaps without cutting through the polyimide substrate with an optimized parameter of power 2%, speed 20%, PPI 500 in vector mode for 2 times. The PDMS layer was cleaned with ethanol and deionized water to remove debris, followed by 30 s of O_2 plasma surface treatment using Plasma Etch PE-25 (10 cm^3 min^{-1} O_2, 100 W, 150 mTorr) to clean its surface and promote surface adhesion. The whole CARES patch was then assembled by dry transferring the top layer onto the bottom layer using a PDMS stamp. Biosensors were prepared before microfluidics integration. Note that the sweat reservoir was pre-defined during 120 μm-thick PDMS middle layer in CARES patch fabrication, which has a dimension of 17.15 mm^2 and thereby a reservoir volume of 2.06 μL. The small volume

allows a fast refreshing rate and enables rapid detection of dynamic changes during human performance.

Microfluidics fabrication: The microfluidics layers were fabricated with a laser cutter layer-by-layer by patterning double-sided M-tape, PET, and PDMS with iontophoresis gel reservoirs, gel electrolytes reservoirs, sweat inlets, flowing channels, and outlets. The optimized laser parameters to cut M-tape were set as power 62%, speed 100%, PPI 500 in vector mode for 2 times, and the optimized parameters to cut PDMS were set as power 2%, speed 20%, PPI 500 in vector mode for 2 times to minimize debris. The iontophoresis gel and gel electrolytes reservoirs were patterned by cutting through all microfluidics layers to define gel area and establish gel connection with skin. The first microfluidics layer is a PDMS-based sweat channel layer, which was spin-coated on a PET petri dish and cured at 60 °C for 1 h. The PDMS layer was treated with O_2 plasma before laminating a thin layer of 12 μm PET, followed by laser-defining sweat inlets. Then the third layer of double-sided M-tape was patterned and aligned onto PET, which contacts with the skin and forms the sweat accumulation layer. After attaching the microfluidics module to the CARES patch, the system was further encapsulated with PDMS backings to avoid potential sweat contact and leakage. The device was connected with a flexible printed circuit (FPC) connector for further characterizations.

Iontophoresis gel fabrication: Both anode and cathode of iontophoresis gel were prepared by mixing agarose (3% w/w) into deionized water and then heated to 250 °C under constant stirring until the solution became homogenous. The solution was then cooled down to 165 °C, during which 1% w/w carbachol and 1% w/w NaCl were added to the anode and cathode solution respectively, and mixed thoroughly. The solution was further cooled down and pooled into the iontophoresis gel reservoirs 41.95 mm^2 for anode and 28.19 mm^2 for cathode respectively. Together with iontophoresis gels, electrolyte gel (SignaGel, Parker laboratories, INC.) was casted onto the GSR electrodes before placing the CARES device on human subjects.

Biosensors preparation and characterization

Enzymatic sensor preparation: An electrochemical workstation (CHI 760E, CH Instruments, USA) was used to prepare enzymatic biosensors. Pulsed voltammetry from −0.9 V to 0.9 V (3000 cycles in total) in 50 mM $HAuCl_4$ was used to deposit Au nanoparticles (AuNPs) on the carbon electrode at a signal frequency of 50 Hz, in order to increase surface area and enhance sensitivity. A thin Prussian blue transducer layer was deposited by applying cyclic voltammetry for 2 cycles for glucose and UA, and 4 cycles for lactate (from −0.2 V to 0.6 V with a scan rate of 50 mV s^{-1}) in a fresh solution consisting of 2.5 mM $FeCl_3$, 2.5 mM $K_3Fe(CN)_6$, 100 mM KCl and 100 mM HCl. The electrodes were then deposited with a nickel hexacyanoferrate (NiHCF) protection layer by applying cyclic voltammetry for 50 cycles (from 0V to 0.8 V with a scan rate of 100 mV s^{-1}) in a fresh solution containing 0.5 mM $NiCl_2$, 0.5 mM $K_3Fe(CN)_6$, 100 mM KCl and 100 mM HCl. The electrodes were then dried before drop-casting enzyme cocktail. For all three amperometric enzymatic sensors, the enzyme cocktails were prepared as follows: BSA (1% w/w), 2.5% glutaraldehyde (2% v/v), and 10 mg mL^{-1} enzyme (4% v/v) was mixed in 1 mL

PBS. 0.5 μL enzyme cocktail was drop-casted onto each enzymatic sensor electrode surface and then dried at 4 °C overnight. For the lactate sensor, a limit diffusion membrane was further drop-casted by applying 0.5 μL solution containing 17 mg PVC and 65 mg DOS in 660 μL THF.

Reference electrode preparation: To prepare the shared reference electrode, 10 μL of 0.1 M $FeCl_3$ solution was drop-casted onto the Ag surface for 20 s and rinsed with deionized water, and then 1.5 μL of PVB reference cocktail was applied on the Ag/AgCl surface by dissolving 79.1 mg PVB and 50 mg NaCl into 1 mL methanol and left drying overnight.

ISE sensors preparation: The Na^+ selective cocktail was prepared as follows: 1 mg of Na ionophore X, 0.55 mg Na-TFPB, 30 mg PVC, 30 mg SEBS, and 65 mg DOS were dissolved in 660 μL THF. The K^+ selective cocktail was prepared as follows: 2 mg of valinomycin, 0.5 mg NaTPB, 30 mg PVC, 25 mg SEBS, and 70 mg DOS were dissolved in 350 μL THF. The NH_4^+ selective cocktail was prepared as follows: 1 mg of nonactin, 30 mg PVC, 30 mg SEBS, and 65 mg DOS were dissolved in 660 μL THF. The inkjet carbon electrode was activated in 0.5 M HCl with cyclic voltammetry scans of 10 cycles (−0.1 V to 0.9 V with a scan rate of 100 mV s^{-1}). The electrodes were then baked in a vacuum oven at 120 °C for 1 hour to remove moisture. 2 μL of Na^+ selective cocktail, 2 μL of K^+ selective cocktail, and 2 μL of NH_4^+ selective cocktail was drop-casted onto the carbon electrode and dried overnight.

In vitro sensor characterization: To obtain the best performance for long-term continuous measurements, all sensors were placed in a buffered solution containing 100 μM glucose, 5 mM lactate, 25 μM UA, 40 mM NaCl, 8 mM KCl, 2 mM NH_4Cl for 30 minutes to minimize the potential drift. All the *in vitro* biosensor characterizations were performed with cyclic voltammetry and amperometric i-t through a multi-channel electrochemical workstation (CHI 1430, CH Instruments, USA). For in vitro enzymatic sensor characterizations, analyte solutions were prepared in PBS, with glucose ranging from 0–100 μM, lactate ranging from 0–20 mM, and UA ranging from 0–100 μM. For in vitro ISE sensor characterizations, analyte solutions were prepared in deionized water, with NaCl ranging from 10–160 mM, KCl ranging from 2–32 mM, NH_4Cl ranging from 0.5–8 mM. The enzymatic sensors were characterized chronoamperometrically at a potential of 0 V, and ISE sensors were characterized using open circuit potential measurement. Both potentiometric and chronoamperometric responses were set as 1 s sampling interval, except for long-term monitoring where the sampling interval was set as 10 s to minimize data overload. To test the pH influence on PB-NiHCF-based enzymatic biosensors, McIlvaine buffer solutions were prepared and calibrated containing 0–100 μM H_2O_2. Temperature influence characterizations were carried out on a ceramic hot plate (Thermo Fisher Scientific).

To characterize the stability of the PB and PB-NiHCF electrodes, dissolved Fe^{2+} concentrations were determined by inductively coupled plasma–mass spectrometry (ICP–MS) using an Agilent 8800. The sample introduction system consisted of a micromist nebulizer, scott type spray chamber and fixed injector quartz torch. A guard electrode was

used and the plasma was operated at 1500 W. All elements were measured in Helium MS/MS mode.

Materials characterization

The morphology of materials was characterized by field-emission scanning electron microscopy (SEM, Nova 600). Cross-sectional lamella was prepared by standard focus ion beam cutting (FIB, Nova 600). The Scanning transmission electron microscopy (STEM) characterizations and energy-dispersive X-ray spectroscopy (EDS) analyses were performed using a JEOL JEM-ARM300CF S/STEM system (300 keV).

Physical sensors characterization

For *in vitro* temperature and GSR sensor characterizations, an amperometric method was used with an applied voltage of 1 V using a dual-channel electrochemical workstation (CHI 760E).

For *in vitro* pulse sensor characterizations, a parameter analyzer (Keithley 4200A-SCS) was applied to record the fast-changing capacitive signals at a sampling frequency of around 137 Hz. The influence of mechanical deformation on the physical sensor performance was investigated through pressing-releasing for 5,000 cycles using a Mark-10 force gauge. The influence of humidity was investigated by immersing the subject hand with the CARES in a customized glove box with a humidity gauge.

Microfluidics evaluation

On-body flow tests were conducted to evaluate the sweat flow of dual-reservoir designs. An assembled microfluidic patch pre-deposited with black dye in the sweat reservoir was attached to a subject's forearm, followed by *in situ* sweat induction using iontophoresis.

Experimental flow tests were also conducted to evaluate the dynamic response of sensors using a syringe pump (78-01001, Thermo Fisher Scientific). Different fluids were injected into the pre-assembled CARES device with a varying flow rate of 1–4 μL min^{-1} (Supplementary Fig. 22).

On-body evaluation of CARES for long-term continuous monitoring

Subject recruitment: The validation and evaluation of the CARES device were performed on healthy human subjects in compliance with the protocols (#19-0892 and #19-0895) that were approved by the Institutional Review Board (IRB) at the California Institute of Technology (Caltech). Participating subjects were recruited from the Caltech campus and the neighboring communities through advertisement by posted notices, word of mouth, and email distribution. 10 healthy subjects (8 males and 2 females, age range 23–38 years) were included in this study. The participants were healthy without anxiety nor depression issues. All subjects gave written informed consent before participation in the study. The study was fully voluntary, and no compensation was given.

On-body protocols: The CARES was mounted on the subject's wrist after skin cleaning with alcohol wipes. Participants were requested to refrain from meals, alcohol, caffeine, and

exercise within 3 h prior to the tests. The CARES was sealed in PDMS, leaving output pins exposed with an M-tape backing as support for wire connections. We further designed a plug-and-play input-output to connect with the flexible flat cable (Supplementary Fig. 41). A 50-μA current was implemented on both pairs of iontophoresis electrodes for 5 minutes simultaneously for sweat induction. The data was collected with an 8-channel multiplexer (CHI Instrument 1430) and a Keithley 4200A-SCS parameter analyzer. A wireless wearable CARES system was also developed for convenient data collection in the real-life settings.

Long-term multimodal sensor evaluation during daily activities: A 24-hour continuous monitoring of physiological and biochemical signals was recorded *via* the CARES device. 5-minute periodical iontophoresis sweat induction was performed at 7 am, 9:30 am, 12:30 pm, 4:00 pm, 7:00 pm, 11:00 pm, 1:30 am, and 4:30 am. The physiological data was collected continuously while data from the biosensors were collected 10 minutes after iontophoresis.

Questionnaire for state anxiety evaluation: State-Trait Anxiety Inventory Form Y (STAI-Y) is a self-evaluation questionnaire that consists of two forms Y-1 and Y-2 to measure state and trait anxiety respectively, which has a high internal consistency coefficient of 0.91–0.93 for college students and working adults[48]. In our study, we used short form Y-1, which measures state anxiety, as a key psychological response to stress. This measure can be proctored during real-time experiments without major intervention during the stress event. One challenge for quantifying stress is the subjective nature of the questionnaire, which inherently holds a small fluctuations of a couple stress points, with a standard deviation of more than 4 points in most cases[48]. In our study, we take ±2 points as the confidence interval buffer for state anxiety level evaluation.

Stressor #1: cold pressor test (CPT): The participants were asked to wear the CARES and to relaxation for 10 minutes after iontophoresis sweat induction, during which no sensor signals were collected. After the relaxing stage, both physical and biosensors started monitoring simultaneously as baseline vital and molecular data. The STAI-Y questionnaire was administered to assess state anxiety levels during this relaxed baseline state. The subject was asked to relaxation for another 1000 s, after which a 3-minute CPT was conducted. Subjects were asked to immerse their other hand without the CARES device into a tank containing iced water (0 °C) up to the forearm for 3 minutes. Another STAI-Y questionnaire was then given to evaluate the state anxiety levels and the subjects were asked to finish within 20 s. Afterward, the subjects were instructed to remove the hand from the iced water, and recover in ambient air. Continuous monitoring of multimodal physiological and biochemical data was monitored throughout the stress challenge and recovery stage until 1000 s after the CPT was finished. The subjects were seated during the whole procedure.

Stressor #2: virtual reality test (VR): The sensor data recording process was the same as aforementioned, except that the subjects were asked to play a VR game (Beat Saber) by wearing a VR headset (Oculus Quest 2, Meta). The game was set as one-handed mode with expert difficulty, and the game screen was projected onto a monitor. The subjects were strongly encouraged verbally and asked to compete with other participants' record

scores, so that a mixed physical and psychological stress could be stimulated. The STAI-Y questionnaire was used to assess state anxiety levels.

Stressor #3: exercise: For exercise-induced stress, the sensor data recording process was the same as aforementioned. The subject performed the maximum-load cycling (>70 rpm) on a stationary exercise bike (Kettler Axos Cycle M-LA) for 3 minutes or until fatigue, during which strong verbal encouragement was given. The STAI-Y questionnaire was used to assess state anxiety levels.

Data collection in real life activities: The subject was asked to perform in-door activities, including relaxation on the phone, playing a long-term VR game (Superhot VR) by wearing a VR headset, and reading journal papers. The subject then performed outdoor activities, including running and walking recovery. The STAI-Y questionnaire was used to assess state anxiety levels during each activity.

Machine learning (ML) pipeline for stress assessment

Data preprocessing and feature extraction: While all the multimodal sensor signals were monitored in real-time, the data pre-processing was performed asynchronously to extract features. A pulse feature extraction algorithm was developed due to its unique peripheral pulse sampling frequency of T = 0.007 s. To match other sensors sampling frequency of T = 1s, each pulse waveform was autonomously analyzed through our pulse analysis algorithm, with a floor function afterwards to select the closest pulse feature within each time interval. Signals of the biochemical sensors were manually shifted by 300 s to align with physical ones due to natural sweat delay; heart rate data in figure plots were extracted from the pulse features and smoothed by the moving average of 100 s to show the trends more clearly. The time stamp when each subject express stress was recorded and manual data labeling was performed. To minimize the variations for inter-subject response, all features were normalized before ML pipeline in regards to each subject during each stress test, in order to generalize the model among population. After data collection and analysis, the training and testing datasets were shuffled and divided 8:2 respectively and were randomly selected using an equal representation of each class. ML model was developed to link the biological and chemical features to the stress detection, stress types, as well as state anxiety levels from questionnaire scores.

Model selection for stress classification: All training model were built using Python (Python 3.8) based on the data collected from ten subjects facing three different stressors with a set of 60,000 s of CARES recordings. Segmentation of the sensor signals was done using a sliding window with a sampling interval of 1 s, given each stress type representation. A number of ML models were evaluated according to precision-recall curve and their F_1 score, including linear and radial basis function (RBF) support vector machines (SVM), logistic and ridge regression, conventional decision trees, as well as gradient-boosted decision tree XGBoost model. The trained XGBoost model outperformed typical ML models for both stress detection and stress type classification.

Model selection for stress regression: The machine learning algorithms were developed on a password-protected local computer with individual GPU module Nvidia 3080. The training model were built as aforementioned, except that the kernel was changed to regressor instead of classifier. For overall stress level evaluations, on the other hand, features were extracted from stress region by taking average signal changes from the moving average (MA) of sensors rather than segmented at each timepoint, and simpler ML models such as linear regression and SVM were evaluated due to the reduced size of dataset to prevent overfitting. A brute force examination of features was performed to compare the contributions of physicochemical biomarkers.

Supplementary Material

Refer to Web version on PubMed Central for supplementary material.

Acknowledgement

This work was funded by the Translational Research Institute for Space Health through NASA NNX16AO69A, Office of Naval Research grants N00014-21-1-2483 and N00014-21-1-2845, Army Research Office grant W911NF-23-1-0041, National Institutes of Health grants R01HL155815, R21DK13266, National Science Foundation grant 2145802, National Academy of Medicine Catalyst Award, High Impact Pilot Research Award T31IP1666 from Tobacco-Related Disease Research Program, and Heritage Medical Research Institute (all to W.G.). T.K.H. acknowledge the support from National Institutes of Health grants T32HL144449 and T32EB027629. C.X. acknowledge the support from Amazon AI4Science Fellowship. ICP-MS instrumentation at the Resnick Sustainability Institute's Water and Environment Lab at the California Institute of Technology with the assistance of Dr. Nathan Dalleska was used in this work. We gratefully acknowledge critical support and infrastructure provided for this work by the Kavli Nanoscience Institute at Caltech, and Center for Transmission Electron Microscopy at University of California Irvine, and we gratefully thank Dr. Matthew Hunt and Dr. Mingjie Xu for their help.

Data availability

All data supporting the results in this study are available in the paper and its supplementary materials. The multimodal data collected by CARES from the human subjects is available at https://github.com/CARES-eskin/StressData.

References

1. Kivimäki M, Bartolomucci A & Kawachi I The multiple roles of life stress in metabolic disorders. Nat. Rev. Endocrinol 19, 10–27 (2022). [PubMed: 36224493]
2. Schneiderman N, Ironson G & Siegel SD STRESS AND HEALTH: Psychological, Behavioral, and Biological Determinants. Annu. Rev. Clin. Psychol 1, 607–628 (2005). [PubMed: 17716101]
3. Kumar A, Rinwa P, Kaur G & Machawal L Stress: Neurobiology, consequences and management. J. Pharm. Bioallied Sci 5, 91–97 (2013). [PubMed: 23833514]
4. Podsakoff NP, Freiburger KJ, Podsakoff PM & Rosen CC Laying the Foundation for the Challenge–Hindrance Stressor Framework 2.0. Annu. Rev. Organ. Psychol. Organ. Behav 10, 165–199 (2023).
5. Pfefferbaum B & North CS Mental health and the COVID-19 pandemic. N. Engl. J. Med 383, 510–512 (2020). [PubMed: 32283003]
6. Santomauro DF et al. Global prevalence and burden of depressive and anxiety disorders in 204 countries and territories in 2020 due to the COVID-19 pandemic. The Lancet 398, 1700–1712 (2021).
7. Gutshall CL, Hampton DP, Sebetan IM, Stein PC & Broxtermann TJ The effects of occupational stress on cognitive performance in police officers. Police Pract. Res 18, 463–477 (2017).

8. Tomporowski PD Effects of acute bouts of exercise on cognition. Acta Psychol. 112, 297–324 (2003).
9. Martin K et al. The impact of environmental stress on cognitive performance: A Systematic Review. Hum. Factors 61, 1205–1246 (2019). [PubMed: 31002273]
10. Robinson SJ, Leach J, Owen-Lynch P. Jane & Sünram-Lea SI Stress reactivity and cognitive performance in a simulated firefighting emergency. Aviat. Space Environ. Med 84, 592–599 (2013). [PubMed: 23745287]
11. Haines MM, Stansfeld SA, Job RFS, Berglund B & Head J Chronic aircraft noise exposure, stress responses, mental health and cognitive performance in school children. Psychol. Med 31, 265–277 (2001). [PubMed: 11232914]
12. Kulshreshtha A et al. Association of stress with cognitive function among older black and white US adults. JAMA Netw. Open 6, e231860 (2023). [PubMed: 36881411]
13. Epel ES et al. More than a feeling: A unified view of stress measurement for population science. Front. Neuroendocrinol 49, 146–169 (2018). [PubMed: 29551356]
14. Thapar A, Eyre O, Patel V & Brent D Depression in young people. The Lancet 400, 617–631 (2022).
15. Topol E Deep Medicine: How Artificial Intelligence Can Make Healthcare Human Again. (Basic Books, Inc., 2019).
16. Herrman H et al. Time for united action on depression: a Lancet–World Psychiatric Association Commission. The Lancet 399, 957–1022 (2022).
17. Drew DA et al. Rapid implementation of mobile technology for real-time epidemiology of COVID-19. Science 368, 1362–1367 (2020). [PubMed: 32371477]
18. Charmandari E, Tsigos C & Chrousos G Endocrinology of the stress response. Annu. Rev. Physiol 67, 259–284 (2005). [PubMed: 15709959]
19. Dolan RJ Emotion, cognition, and behavior. Science 298, 1191–1194 (2002). [PubMed: 12424363]
20. Harker M Psychological sweating: Psychological sweating: A systematic review focused on aetiology and cutaneous response. Skin Pharmacol. Physiol 26, 92–100 (2013). [PubMed: 23428634]
21. Axelrod J & Reisine TD Stress hormones: Their interaction and regulation. Science 224, 452–459 (1984). [PubMed: 6143403]
22. Acosta JN, Falcone GJ, Rajpurkar P & Topol EJ Multimodal biomedical AI. Nat. Med 28, 1773–1784 (2022). [PubMed: 36109635]
23. Buergel T et al. Metabolomic profiles predict individual multidisease outcomes. Nat. Med 28, 2309–2320 (2022). [PubMed: 36138150]
24. Ates HC et al. End-to-end design of wearable sensors. Nat. Rev. Mater 7, 887–907 (2022). [PubMed: 35910814]
25. Wang C et al. Bioadhesive ultrasound for long-term continuous imaging of diverse organs. Science 377, 517–523 (2022). [PubMed: 35901155]
26. Kim D-H et al. Epidermal electronics. Science 333, 838–843 (2011). [PubMed: 21836009]
27. Xu C, Yang Y & Gao W Skin-interfaced sensors in digital medicine: from materials to applications. Matter 2, 1414–1445 (2020). [PubMed: 32510052]
28. Niu S et al. A wireless body area sensor network based on stretchable passive tags. Nat. Electron 2, 361–368 (2019).
29. Gao W et al. Fully integrated wearable sensor arrays for multiplexed *in situ* perspiration analysis. Nature 529, 509–514 (2016). [PubMed: 26819044]
30. Wang M et al. A wearable electrochemical biosensor for the monitoring of metabolites and nutrients. Nat. Biomed. Eng 6, 1225–1235 (2022). [PubMed: 35970928]
31. Kim J, Campbell AS, de Ávila BE-F & Wang J Wearable biosensors for healthcare monitoring. Nat. Biotechnol 37, 389–406 (2019). [PubMed: 30804534]
32. Ray TR et al. Bio-integrated wearable systems: A comprehensive review. Chem. Rev 119, 5461–5533 (2019). [PubMed: 30689360]

33. Chesnut M et al. Stress markers for mental states and biotypes of Ddepression and anxiety: A scoping review and preliminary illustrative analysis. Chronic Stress 5, 24705470211000338 (2021). [PubMed: 33997582]
34. Xu S, Kim J, Walter JR, Ghaffari R & Rogers JA Translational gaps and opportunities for medical wearables in digital health. Sci. Transl. Med 14, eabn6036 (2022). [PubMed: 36223451]
35. Torrente-Rodríguez RM et al. Investigation of cortisol dynamics in human sweat using a graphene-based wireless mHealth system. Matter 2, 921–937 (2020). [PubMed: 32266329]
36. Wang B et al. Wearable aptamer-field-effect transistor sensing system for noninvasive cortisol monitoring. Sci. Adv 8, eabk0967 (2022). [PubMed: 34985954]
37. Sheibani S et al. Extended gate field-effect-transistor for sensing cortisol stress hormone. Commun. Mater 2, 10 (2021). [PubMed: 33506228]
38. Simmers P, Li SK, Kasting G & Heikenfeld J Prolonged and localized sweat stimulation by iontophoretic delivery of the slowly-metabolized cholinergic agent carbachol. J. Dermatol. Sci 89, 40–51 (2018). [PubMed: 29128285]
39. Sancini A & Tomei F Work related stress and blood glucose levels. Ann. Ig 29, 123–133 (2017). [PubMed: 28244581]
40. Hermann R, Lay D, Wahl P, Roth WT & Petrowski K Effects of psychosocial and physical stress on lactate and anxiety levels. Stress 22, 664–669 (2019). [PubMed: 31062999]
41. Kubera B et al. Rise in plasma lactate concentrations with psychosocial stress: A possible sign of cerebral energy demand. OFA 5, 384–392 (2012).
42. Klous L, de Ruiter CJ, Scherrer S, Gerrett N & Daanen HAM The (in)dependency of blood and sweat sodium, chloride, potassium, ammonia, lactate and glucose concentrations during submaximal exercise. Eur. J. Appl. Physiol 121, 803–816 (2021). [PubMed: 33355715]
43. Goodman AM et al. The hippocampal response to psychosocial stress varies with salivary uric acid level. Neuroscience 339, 396–401 (2016). [PubMed: 27725214]
44. Nyein HYY et al. A wearable electrochemical platform for noninvasive simultaneous monitoring of Ca^{2+} and pH. ACS Nano 10, 7216–7224 (2016). [PubMed: 27380446]
45. Lin S et al. Wearable microneedle-based electrochemical aptamer biosensing for precision dosing of drugs with narrow therapeutic windows. Sci. Adv 8, eabq4539 (2022). [PubMed: 36149955]
46. Tu J et al. A wireless patch for the monitoring of C-reactive protein in sweat. Nat. Biomed. Eng 7, 1293–1306 (2023). [PubMed: 37349389]
47. Shao Y, Ying Y & Ping J Recent advances in solid-contact ion-selective electrodes: functional materials, transduction mechanisms, and development trends. Chem. Soc. Rev 49, 4405–4465 (2020). [PubMed: 32458836]
48. Spielberger C Manual for the state-trait anxiety inventory (STAI Form Y). Consulting Psychologists Press, Inc. (1983).
49. Frank SM & Raja SN Reflex cutaneous vasoconstriction during cold pressor test is mediated through α-adrenoceptors. Clin. Auton. Res 4, 257–261 (1994). [PubMed: 7888745]
50. Schwabe L, Haddad L & Schachinger H HPA axis activation by a socially evaluated cold-pressor test. Psychoneuroendocrinology 33, 890–895 (2008). [PubMed: 18403130]
51. Khambam SKR, Naidu MUR, Rani PU & Rao TRK Effect of cold stimulation-induced pain on pharmacodynamic responses in healthy human volunteers. Int. J. Nutr. Pharmacol. Neurol. Dis 2, 26 (2012).
52. Buono MJ, Lee NVL & Miller PW The relationship between exercise intensity and the sweat lactate excretion rate. J. Physiol. Sci 60, 103–107 (2010). [PubMed: 20013328]
53. van der Maaten L & Hinton G Visualizing data using t-SNE. J Mach. Learn. Res 9, 2579–2605 (2008).
54. Hay Elizabeth L. & Diehl Manfred. Reactivity to daily stressors in adulthood: The importance of stressor type in characterizing risk factors. Psychol. Aging 25, 118–131 (2010). [PubMed: 20230133]
55. Crestani CC Emotional stress and cardiovascular complications in animal models: A review of the influence of stress type. Front. Physiol 7, (2016).

56. Pow J, Lee-Baggley D & DeLongis A Threats to communion and agency mediate associations between stressor type and daily coping. Anxiety, Stress, & Coping 29, 660–672 (2016). [PubMed: 26652309]

57. A Handbook for the Study of Mental Health: Social Contexts, Theories, and Systems. (Cambridge University Press, 2009). doi:10.1017/CBO9780511984945.

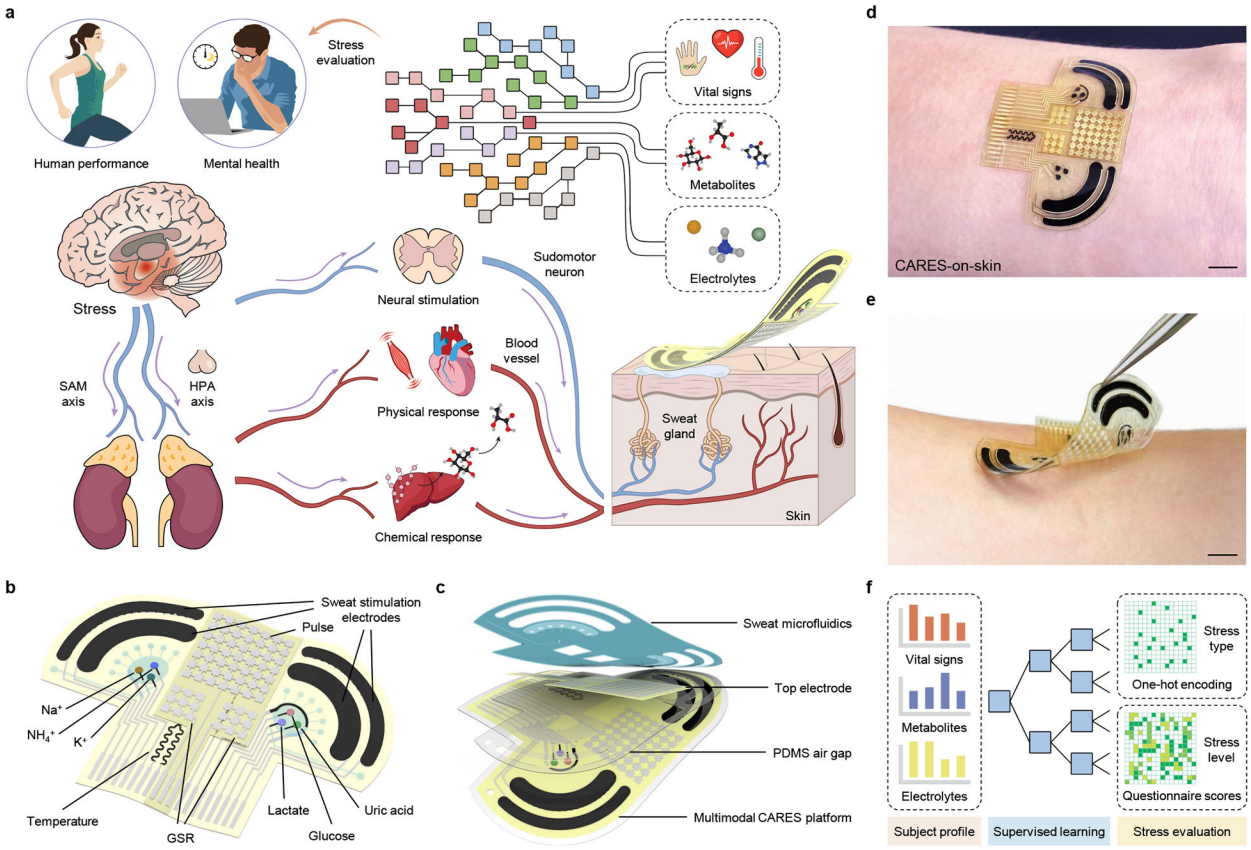

Fig. 1 | A consolidated artificial intelligence-reinforced electronic skin (CARES) for stress response monitoring.

a, Illustration of the CARES that continuously monitors multimodal physiological and biochemical response from skin, and performs artificial intelligence (AI)-powered stress assessment. HPA, hypothalamic-pituitary-adrenal; SAM, sympathetic-adreno-medullar. **b**, Schematic of the flexible CARES sensor patch and main functionalities: vital sign monitoring, sweat stimulation and sampling, and key metabolite and electrolyte detection. **c**, Schematic of layered structure of the CARES that assembles sensor and microfluidics module. **d**,**e**, Optical images of a CARES attached to the skin of a human subject. Scale bars, 1 cm. **f**, Machine learning (ML) pipeline for CARES-enabled stressor classification and stress/anxiety level assessment.

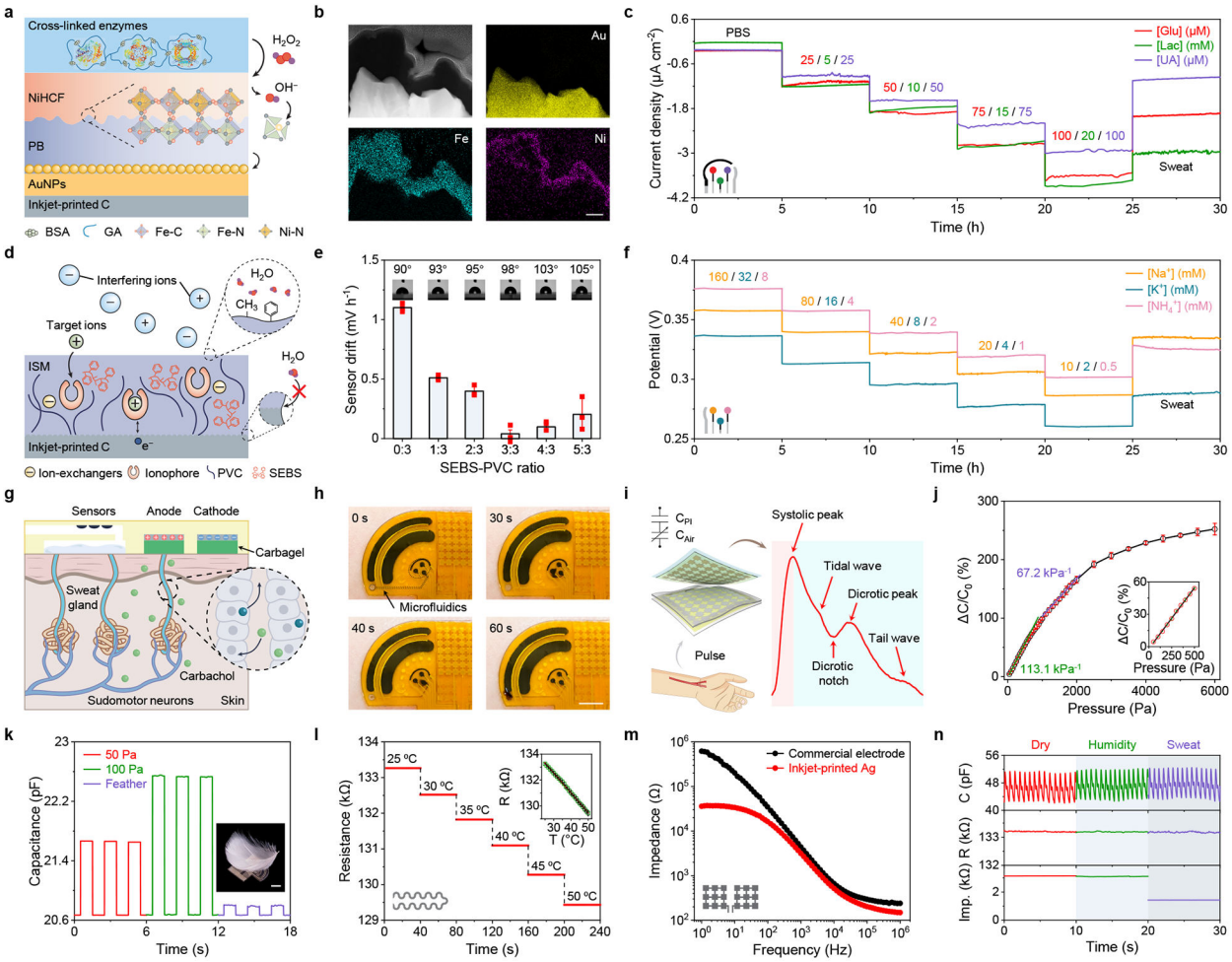

Fig. 2 | Design and characterization of highly robust multimodal sensors.

a, Mechanism of enzymatic metabolite sensors. PB, Prussian blue; NiHCF, nickel hexacyanoferrate; AuNPs, gold nanoparticles; GA, glutaraldehyde. **b**, Cross-sectional STEM and EDS images of the PB-NiHCF interface. Scale bar, 100 nm. **c**, Operational long-term stability of enzymatic glucose, lactate, and uric acid (UA) sensors in phosphate buffered saline (PBS) and sweat samples for 30 hours. Glu, glucose; Lac, lactate. **d**, Mechanism of ion-selective electrolyte sensors. ISM, ion-selective membrane; PVC, polyvinyl chloride; SEBS, polystyrene-block-poly (ethylene butylene)-block-polystyrene. **e**, SEBS-PVC ratios in regards to sensor stability. Insets, contact angle measurements for different SEBS ratios. Data is presented as mean ± SD (n = 3 sensors). **f**, Operational long-term stability of ion-selective Na^+, K^+ and NH_4^+ sensors in standard solutions and sweat samples for 30 hours. **g**,**h**, Schematic (**g**) and on-body evaluation (**h**) of the microfluidic iontophoresis module for autonomous sweat induction and sampling at rest. Timestamps in **h** represent the period after a 5-min iontophoresis session. **i**, Schematic of the pressure sensor and a pulse waveform measured at the wrist. PI, polyimide. **j**, Pressure versus capacitance (C) characterizations of the pressure sensor. C_0, flat-state C. Data is presented as mean ± SD (n = 3 sensors). **k**, Repetitive response of the pressure sensor upon small pressure loads. Inset, a goose feather placed on a sensor. Scale bar, 1 cm. **l**, Response of the temperature (T) sensor

in the physiological temperature range. R, resistance. **m**, Impedance of the skin/electrode interface measured with inkjet-printed Ag electrodes and commercial electrodes for galvanic skin response (GSR) monitoring. **n**, Performance of encapsulated pulse, T and GSR sensors under environmental humidity and body sweat test. All error bars represent the SD from three sensors.

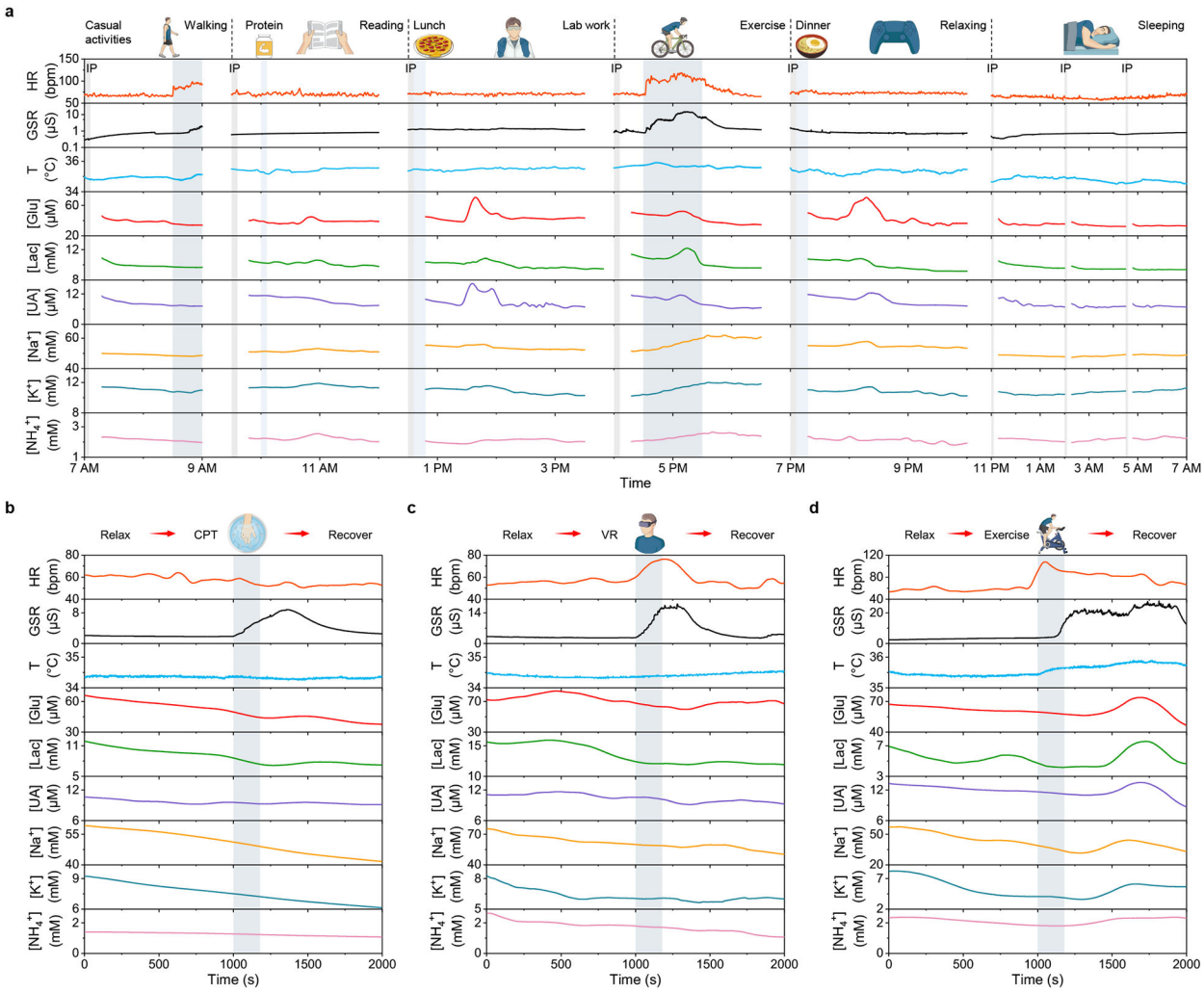

Fig. 3 |. On-body evaluation of the CARES in daily activities and under various types of physiological and psychological stressors.

a, Continuous 24-hour multimodal monitoring during a subject's daily activities. IP, iontophoresis; HR, heart rate; bpm, beats per minute. **b**–**d**, Multimodal monitoring of a selected subject's stress response under three different stressors: cold pressor test (CPT) (**b**) during which the subject was asked to immerse one hand into ice water, virtual reality challenge (VR) (**c**) during which the subject was asked to play a VR rhythm game, and cycling exercise test (**d**) during which the subject was asked to perform a maximum-load cycling challenge on a stationary exercise bike.

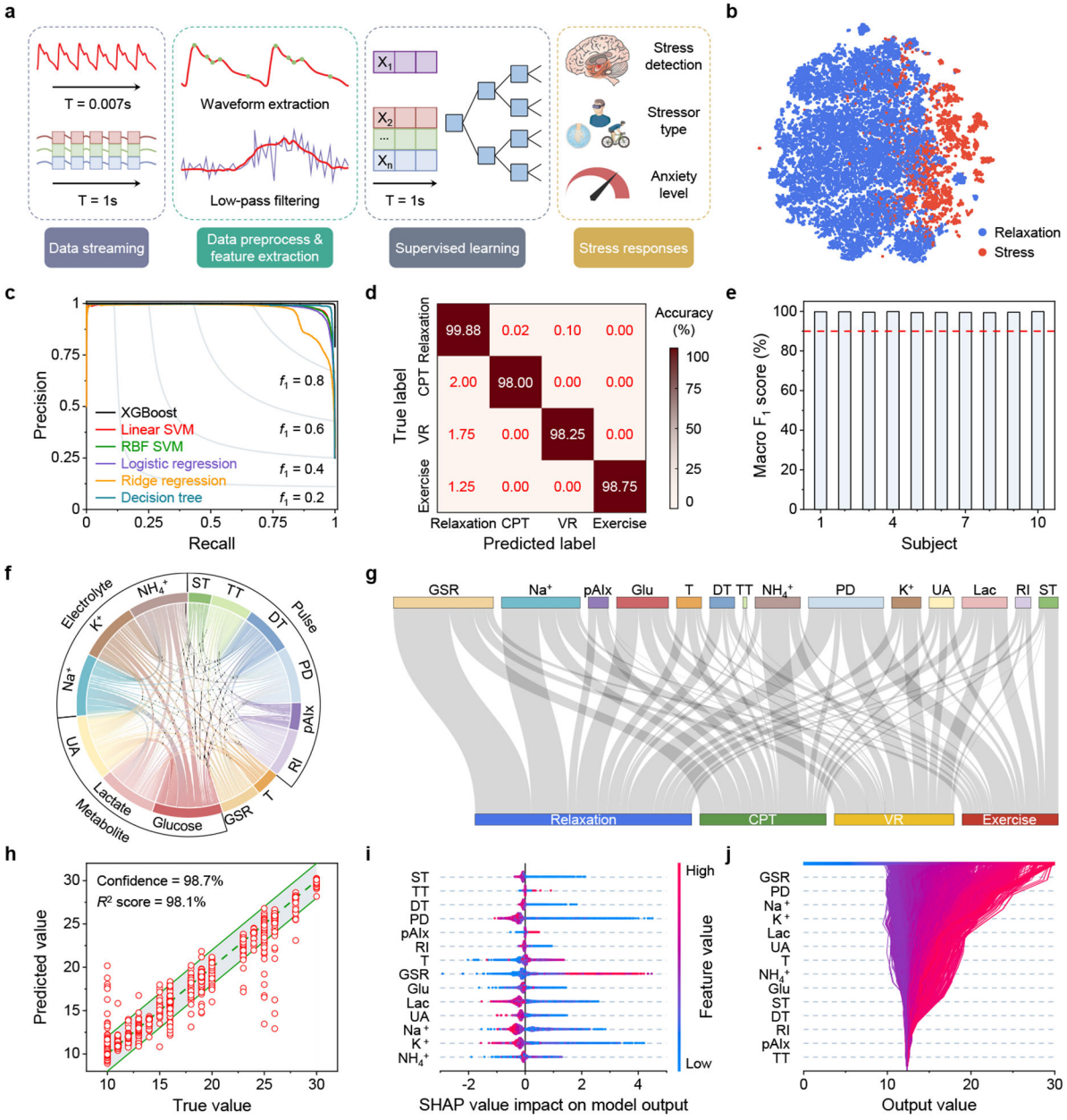

Fig. 4 | ML-powered stress response assessment.

a, Schematics of the ML architecture for data preprocessing, feature extraction, supervised learning and evaluation. **b**, t-distributed stochastic neighbor embedding (t-SNE) plot from the dataset recorded by the CARES visually showing feature separation in a 2-dimensional space. **c**, Precision-recall curve of different ML models for stressor classification. XGBoost, extreme gradient boosting; SVM, support vector machine; RBF, radial basis function. **d**, Confusion matrix displaying the classification accuracy for predicting each type of stressor in test set. **e**, The overall stress classification accuracy based on macro-averaged F_1 score for each subject. **f**, A chord diagram showing the relative correlation between different sensors. ST, systolicTime; TT, tidalPeakTime; DT, dicroticPeakTime; PD, pulseDuration; pAIx, peripheral augmentation index; RI, reflectionIndex. **g**, Sankey diagram of SHAP

analysis depicting the relative contribution of different sensors to stressor classification. **h**, True versus the ML-predicted state anxiety scores. Data is presented as ±2 state anxiety score buffer based on the potential error in the anxiety questionnaires. **i**, Shapley additive explanation (SHAP) summary plot for state anxiety level evaluation based on the dataset collected by the CARES. Each axis plots the distribution of SHAP values of a given feature for each prediction instance. **j**, SHAP decision plot explaining how the ML model determines the state anxiety level using both physiological and biochemical features.